X-ray standing wave analysis of the Sn/Si(111)-$\sqrt{3}\times\sqrt{3}$ surface

A. A. Escuadro,[1] D. M. Goodner,[1] J. S. Okasinski,[1] and M. J. Bedzyk[1,2]
[1]*Department of Materials Science and Engineering, and Materials Research Center, Northwestern University, Evanston, Illinois 60208, USA*
[2]*Materials Science Division, Argonne National Laboratory, Argonne, Illinois 60439, USA*
(Received 8 July 2004; published 15 December 2004)

The 1/3 monolayer (ML) Sn/Si(111)-($\sqrt{3}\times\sqrt{3}$)*R*30° surface structure has been extensively studied using low-energy electron diffraction (LEED) and x-ray standing waves (XSW). The summation of several XSW measured *hkl* Fourier components provides a three-dimensional, model-independent direct-space image of the Sn atomic distribution. While the image demonstrates that the Sn atoms are located at Si(111) T_4-adsorption sites, it alone can not determine whether or not the Sn atomic distribution is flat or asymmetric. However, conventional XSW analysis can make this distinction, concluding that one-third of the Sn atoms are located 0.26 Å higher than the remaining two-thirds. This "one up and two down" distribution result is consistent with the vertical displacements predicted by a dynamical fluctuations model of the surface. For a second sample with a slightly different surface preparation a $\sqrt{3}$ LEED pattern was again observed, but in this case the direct space XSW imaging technique clearly revealed that a significant fraction of the Sn atoms were substituting for Si atoms in the bottom of the Si surface bilayer.

DOI: 10.1103/PhysRevB.70.235416 PACS number(s): 68.43.Fg, 68.35.Rh, 68.49.Uv

I. INTRODUCTION

The atomic scale structure of the 1/3 monolayer (ML) Sn/Si(111)-($\sqrt{3}\times\sqrt{3}$)*R*30° surface (also referred to as "$\sqrt{3}$" surface) has recently attracted attention because of its structural and electronic similarities to the 1/3 ML Sn on Ge(111) surface, which also forms a $\sqrt{3}$ structure at room temperature (RT). It is generally accepted that the main feature of this atomic configuration is the adsorption of 1/3 ML of Sn at the T_4-adsorption sites, as depicted in Fig. 1. Scanning tunneling microscopy (STM) images show that all the Sn adatoms at the T_4 sites appear equivalent at RT, which suggests a flat structure on both Si(111) and Ge(111). However, an interesting difference arises when the semiconductor surfaces are cooled below RT. While the Sn/Si(111) surface maintains the same $\sqrt{3}$ superstructure at low temperature ($\geqslant$6 K),[1] the Sn/Ge(111) surface changes to a (3×3) reconstruction when cooled below its transition temperature of $\sim$210 K.[2] This (3×3) phase is seen in STM images as a vertical "rippling" of the Sn atoms, in which one of the three Sn atoms in the (3×3) unit cell appears from different from the other two.[2] This phase transition has been attributed to a variety of phenomena, including surface charge density waves,[2,3] Ge substitutional defects,[4–8] and temperature dependent dynamical fluctuations,[9–12] yet there is little agreement on the dominant driving force for the low temperature (LT) (3×3) reconstruction. It is the unresolved nature of this phase transition on Sn/Ge(111), as well as its apparent absence in the case of Sn/Si(111), that has motivated the recent interest in these complementary semiconductor surfaces.

A recent x-ray standing wave (XSW) study on the 1/3 ML Sn/Ge(111) surface concluded that the time-averaged Sn atomic distribution (as projected into the Ge primitive unit cell) remains constant at RT and LT despite the different surface reconstructions observed with low-energy electron diffraction (LEED) and STM.[13] For the RT $\sqrt{3}$ phase, it was determined that the Sn local configuration was incompatible with the expected symmetric distribution, but instead was indicative of the asymmetric LT (3×3) atomic distribution. It was determined that both the RT and LT surface structure consists of three Sn atoms in a (3×3) unit cell occupying two distinct positions in a regular "one up, two down" configuration. This observation lends support to the dynamical fluctuations model for the Sn/Ge(111) surface, in which the Sn atoms rapidly fluctuate between two distinct vertical positions at RT, but are frozen into a 3×3 configuration at LT (i.e., a 2D order-disorder phase transition).

Because of the similarity between Ge and Si, it is possible that the 1/3 ML Sn/Si(111) surface would also follow a similar dynamical fluctuations model. Evidence for this model is found in core-level photoemission spectra of (3×3) and $\sqrt{3}$ Sn/Ge(111) (Refs. 9, 14, and 15) and $\sqrt{3}$ Sn/Si(111),[16–19] which all display a Sn 4*d* line shape that is composed of two components with an intensity ratio of approximately 2:1. Valence-band photoemission studies on Sn/Ge(111) (Refs. 9, 14, and 15) and Sn/Si(111) (Refs. 19–21) also indicate a surface band splitting that is unexpected for a symmetric $\sqrt{3}$ structure. The reported core-level and valence-band measurements were conducted at RT, as well as at a variety of lower temperatures [70 K (Refs. 14 and 19), 100 K (Ref. 15), and 170 K (Ref. 21)]. These electronic results suggest two types of Sn are present in each of these surfaces, with each type having a unique chemical and atomic environment. The fact that both types of Sn are present at RT in Sn/Si(111) can be naturally explained in the dynamical fluctuations model. However, this view has been disputed in a STM and LEED investigation of 1/3 ML Sn/Si(111), which found no evidence of any (3×3) symmetry at temperatures as low as 6 K.[1] Density functional theory calculations, however, suggest a partial softening of a surface phonon can explain the lack of a LT phase transition within the framework of a dynamical fluctuations model.[12] Another

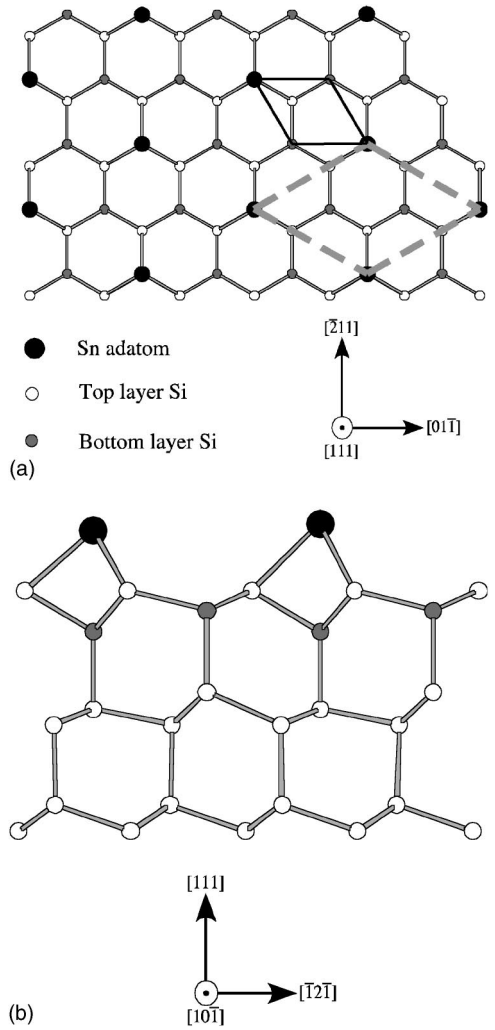

FIG. 1. Ball-and-stick diagram of the 1/3 ML Sn/Si(111) surface. (a) Sn adatoms occupy one-third of the T_4 adsorption sites. The (1×1) surface unit cell is inscribed in a solid black line and the $(\sqrt{3}\times\sqrt{3})$-$R30°$ surface unit cell is inscribed in a dashed gray line. (b) Side view of the Sn/Si(111) surface. Si atoms are displaced from their bulklike positions according to the calculated atomic displacements of Ref. 27.

theoretical study proposed a different type of dynamical model, in which different Sn structural configurations beyond a "one up, two down" arrangement are driven by strain but are obscured by thermal fluctuations.[22] It has been suggested that these configurations may represent a case of dynamical valence fluctuation, in which a classical fluctuating state or a quantum fluctuating state can exist. Clearly, the Sn/Si(111)-$\sqrt{3}$ surface is more complex than expected, and further structural information must be obtained in order to understand these conflicting results.

To that end, we have performed *in situ* Auger electron spectroscopy (AES), LEED, and XSW measurements on 1/3 ML of Sn on Si(111) with the goal of determining the structural details of the Sn/Si(111) surface at RT. By a Fourier summation using the XSW measured Fourier amplitudes and phases, we are able to generate a model-independent image of the Sn time-averaged atomic distribution. While this direct-space image confirms Sn is located at the T_4-adsorption site, it is unable to sufficiently resolve whether there are one or two types of Sn on the surface. However, applying a conventional XSW analysis approach demonstrates that our XSW results are not compatible with a flat $\sqrt{3}$ structure; instead, it points to a structural configuration consisting of Sn adatoms adsorbed at T_4 sites at two distinct heights separated by 0.26 Å in a "one up, two down" arrangement. For a second surface prepared under slightly different conditions, we will also demonstrate a case of a certain fraction of Sn atoms substituting for Si atoms within the subsurface Si layer. This surface proves to be an effective demonstration of the model-independent direct-space imaging approach, since the separation between the Sn adatoms and the subsurface Sn is large enough that it can be easily resolved.

II. EXPERIMENTAL DETAILS

Sample preparation and characterization were conducted in an ultrahigh vacuum (UHV) chamber (base pressure $\sim1.5\times10^{-10}$ Torr) located at the 12ID-D undulator BESSRC-CAT experimental station at the Advanced Photon Source, Argonne National Laboratory. The single-crystal Si(111) samples were cut from a high purity boule of float zone Si with a miscut angle less than 0.1°. After etching, the Si samples were Syton polished to produce a mirrorlike finish. The samples were then degreased, etched using a modified Shiraki process, and then mounted in a strain-free manner on molybdenum sample holders before insertion into the UHV system. The samples were degassed for 6–8 h at 873 K, and then annealed for 15 min at 1113 K to remove the chemically grown protective oxide. AES showed C and O contamination levels to be less than 0.02 ML. The sample temperature during each processing step was measured using an optical pyrometer. The high-temperature anneal produced a clean, well-ordered Si(111)-(7×7) surface, which was confirmed with LEED. A total of 0.33(3) ML of Sn was evaporated onto the clean, RT Si(111) surface at a rate of 0.016 ML/min using an effusion cell. The coverage of Sn was determined in UHV by comparing the intensity of the Sn $L\alpha$ x-ray fluorescence to that of a Sn-implanted Si(111) standard calibrated by Rutherford backscattering spectroscopy. The samples were annealed for 4 min at 913 K (a process which has been noted to result in $\sqrt{3}$ surfaces with a minimal amount of Si substitutional defects),[23] then allowed to slowly cool to RT (at a rate of ~1 K/s). This process resulted in a reduction in the Sn coverage to 0.23(3) ML and a sharp $\sqrt{3}$ LEED pattern.

The XSW measurements were made after allowing the sample to cool to room temperature. The data in Fig. 2 were collected by scanning the sample in angle through the allowed Si(*hhh*) Bragg reflections ($h=1$, 3, 4, and 5) and simultaneously collecting the diffracted beam intensity and x-ray fluorescence spectra [using an *in vacuo* photodiode and energy-dispersive Si(Li) detector, respectively] at each angular step. Three additional off-normal XSW measurements were collected in the same manner utilizing the Si $(\bar{1}11)$, $(\bar{3}33)$, and $(\bar{5}11)$ Bragg reflections in order to determine the

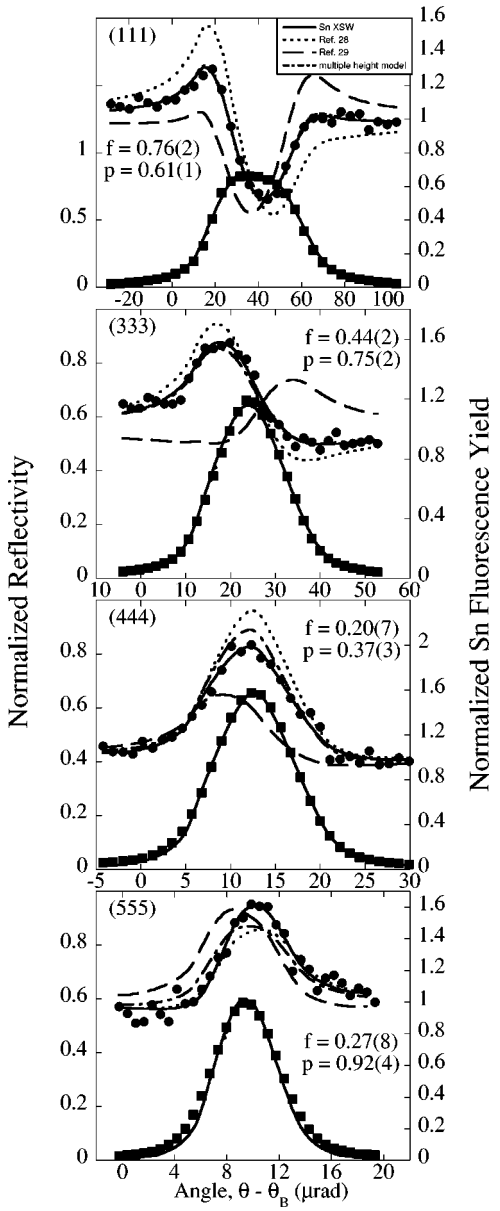

FIG. 2. Reflectivity (closed squares) and normalized Sn $L\alpha$ fluorescence yield (closed circles) experimental data along with theoretical fits (solid lines) for the Si(*hhh*) XSW measurements on 0.23(3) ML Sn/Si(111). Included for comparison are the calculated yield curves based on the results of Profeta *et al.* (dotted line), Yamanaka *et al.* (dashed line), and the proposed structural model (dots plus dashes line).

in-plane Sn distribution. The {111}, {333}, and $(\bar{5}\bar{1}\bar{1})$ XSW measurements were collected using 6.9 keV x-rays that were conditioned by the high-heat-load 12ID Si(111) monochromator. For the {111} XSW measurements, a pair of detuned nondispersive Si(111) channel-cut crystals was used to condition the incident beam; in all other cases, a single *d*-spacing-matched Si(*hhh*) channel cut was used. Because of the particulars of the experimental setup, the higher-order Si(*hhh*) measurements required the use of higher-energy x rays (h=4, 9.4 keV; h=5, 11.2 keV). Fitting the normalized reflectivity and Sn $L\alpha$ fluorescence yield with dynamical diffraction theory produced the coherent position (P_H) and coherent fraction (f_H) for the adsorbed Sn atoms. Any change in the coherent fraction due to the deterioration of the sample over time was monitored by repeating the (111) XSW measurement. Based on a comparison of these two (111) measurements, the fraction of ordered Sn decreased by 7% over a 42 h period. Because the entire XSW experiment was conducted over a period of ~64 h, it is assumed the effect of sample disorder on the other (*hhh*) measurements is small. Finally, in order to ensure the integrity of the data and analysis the bulk Si $K\alpha$ fluorescence was analyzed and found to agree with the expected XSW parameters for the Si substrate.

TABLE I. Summary of the XSW results for the 0.23(3) ML Sn/Si(111) surface. The unit cell origin coincides with the top of the bulklike Si bilayer.

(*hkl*)	P_H	f_H
(111)	0.61(1)	0.76(2)
(333)	0.75(2)	0.44(2)
(444)	0.37(3)	0.20(7)
(555)	0.92(4)	0.27(8)
$(\bar{1}\ 1\ 1)$	0.49(1)	0.89(5)
$(\bar{3}\ 3\ 3)$	0.58(2)	0.36(3)
$(5\ \bar{1}\ \bar{1})$	0.58(2)	0.41(4)

III. RESULTS AND DISCUSSION

The results from the set of XSW measurements are summarized in Table I. The tabulated coherent fractions (f_H) and coherent positions (P_H) are the directly measured amplitudes and phases of the *hkl* Fourier components of the Sn distribution. Because a sufficiently complete set of Fourier coefficients was measured, the collected XSW reciprocal-space data can be Fourier inverted according to the following equation:[24]

$$\rho(\boldsymbol{r}) = \sum_H f_H \exp[-2\pi i(\boldsymbol{H}\cdot\boldsymbol{r} - P_H)]$$
$$= 1 + 2\sum_{H\neq -H\neq 0} f_H \cos[2\pi(P_H - \boldsymbol{H}\cdot\boldsymbol{r})]. \quad (1)$$

The result of this Fourier sum is an element-specific, direct space atomic-density map $\rho(\boldsymbol{r})$. Since the photoelectric effect cross section (in the dipole-approximation) is proportional to the E-field intensity at the center of the atom, the resultant 3D atomic-density map is for the time-averaged locations of the atomic centers. This elemental distribution is generated independently from any presupposed structural constraints, unlike conventional XSW analysis that relies on the comparison of experimental and model-calculated XSW parameters. Since this summation includes only the *hkl* Fourier coefficients that arise from the allowed bulk Bragg reflections, the calculated adsorbate atomic density is necessarily projected into the primitive unit cell of the substrate. Furthermore, because the summation will always be limited to a finite number of measured *hkl* Fourier components, density oscillations

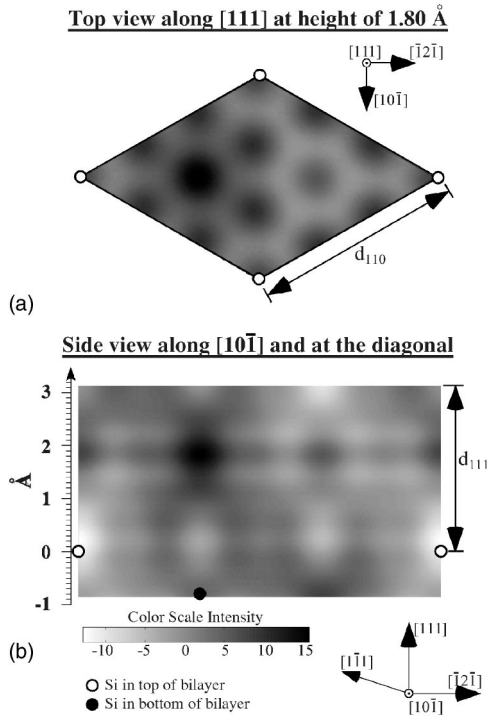

FIG. 3. 2D cuts through the 3D XSW direct space Sn atomic density maps for the 1/3 ML Sn/Si(111) surface. The superstructure is projected into the primitive unit cell of the bulk crystal. The atomic density scale is shown in grayscale and represents the region of maximum Sn atomic density as dark spots. The scale of the atomic density map directly results from evaluating Eq. (1) using the XSW data from Table I. (a) Top view of the (1×1) surface unit cell. (b) Side view of the (1×1) surface unit cell. Both 2D maps are positioned to cut through the maximum of the 3D Sn density map, which coincides with the T_4 adsorption site. The subsidiary maxima surrounding the T_4 site are artifacts due to the termination of the Fourier sum.

will appear in the background of the direct-space map due to the abrupt truncation of the Fourier series. This XSW Fourier reconstruction method has been very recently developed and used to generate one-dimensional impurity atom distributions in bulk crystals[25] and to produce three-dimensional density profiles of adatoms on single crystal surfaces.[13,26]

The direct-space Sn density distribution generated by the measured XSW parameters from Table I is shown in Fig. 3. The resolution limit of this method corresponds to one-half of the smallest *d*-spacing measured, which in this case is $d_{555}/2=0.31$ Å. The top view shown in Fig. 3(a) shows the Sn density variations at a height of 1.80 Å above the Si(111) surface [where the origin is chosen to be the top atom of the bulklike Si(111) bilayer]. This view demonstrates the maximum Sn atom density is centered at the T_4 adsorption site, as expected. This is confirmed by the XSW coherent position measurements agreeing with the relationships $P_{\bar{1}\bar{1}\bar{1}}=(P_{111}+1)/3$ and $P_{\bar{3}\bar{3}\bar{3}}=(P_{333}+1)/3$, which are the geometrical symmetry conditions for the occupation of T_4-adsorption sites on the Si(111) surface.

The side view shown in Fig. 3(b) is a cross-sectional cut through the Sn density distribution containing the long diagonal of the (1×1) surface unit cell. While this view also shows the Sn occupies the T_4-adsorption site, there is no obvious vertical asymmetry or multiple density maxima, as would be expected for Sn adsorbed at multiple heights. This can be interpreted in one of two ways: either the Sn is arranged in a flat, $\sqrt{3}$ structure as seen in STM images, or the Sn is in a "rippled" configuration, but the height separation between Sn adatoms is less than the 0.31 Å resolution of this XSW direct-space image. In order to distinguish between these two possibilities, a comparison between the measured (*hhh*) coherent positions can be made to obtain a qualitative sense of the vertical distribution of the Sn atoms.

If the equilibrium state of the $\sqrt{3}$ surface is composed of Sn atoms at a single height, it would be expected that the measured P_{111} and P_{333} would follow the relationship: $P_{333}=\mathrm{Mod}_1[3P_{111}]$. This relationship will hold if the time-averaged distribution of Sn, as projected along the [111] direction, is symmetric. However, if one compares the results from the (111) and (333) XSW measurements, it can be seen that our measured value for $P_{333}=0.75$ is less than $\mathrm{Mod}_1[3P_{111}]=3(0.61)-1=0.83$, which demonstrates the Sn atomic distribution is not consistent with the single height model developed by earlier structural studies. In fact, relating the measured (111) and (333) coherent positions demonstrates the time-averaged projected Sn distribution is asymmetric and furthermore bottom-heavy. While the additional (*hhh*) XSW parameters will help refine the details of this asymmetric configuration, this simple comparison of two measurements immediately addresses the primary question concerning the 1/3 ML Sn/Si(111) surface structure: whether or not the RT Sn vertical distribution is flat or asymmetric. However, in order to precisely determine the structural details of this asymmetric Sn distribution, an appropriate model for the Sn/Si(111) surface can be employed to interpret the XSW results.

Such a model was developed in the previously mentioned XSW investigation of 1/3 ML Sn/Ge(111). These XSW measurements concluded that the Sn atoms are located at the T_4-adsorption sites and favored a "one up, two down" structure at both RT and at 115 K. These same assumptions detailed in the earlier XSW study can also be used here: (1) one-third of the ordered Sn is located at a height h_A and the remaining two-thirds are at a height h_B, (2) the rms vibrational amplitudes $\langle u^2\rangle^{1/2}$ along the [111] direction for all Sn atoms are identical, and (3) some fraction of Sn $(1-C)$ is randomly distributed, while the remaining fraction C of Sn is located at T_4 sites. As the direct-space images in the previous section show, the assumption that Sn adsorbs at some height above the T_4 sites is a valid one.

In order to relate the measured amplitude (f_H) and phase (P_H) of the Hth Fourier coefficient (F_H) to the model parameters, the following equation is used:

$$F_m = f_m \exp(2\pi i P_m) = C[(1/3)\exp(2\pi i m h_A/d_{111}) + (2/3)\exp(2\pi i m h_B/d_{111})]\exp(-2\pi^2 m^2\langle u^2\rangle/d_{111}^2). \quad (2)$$

In this equation, m refers to the order of the (*hhh*) reflection of interest $(m=1,3,4,5)$. A global chi-squared minimization

routine was used to integrate the four sets of XSW data, account for the relative errors for each individual XSW measurement, and calculate a set of model parameters. The fitting routine resulted in a structural model with a "one up, two down" configuration, with the up position at $h_A = 2.04(5)$ Å above the top of the Si bulklike layer and the down position at $h_B = 1.78(3)$ Å. The vibrational amplitude for the Sn atoms in the [111] direction was calculated to be $\langle u^2\rangle^{1/2} = 0.13(3)$ Å, while the Sn ordered fraction was $C = 0.81(2)$. The reduced chi-squared value for this fit was 1.98.

With the Sn adatoms arranged in the configuration detailed above, the resulting Sn—Si bond length would be 3.01 Å for the top Sn atoms and 2.84 Å for the lower Sn atoms, if Si were located at bulklike positions. These distances, which are 10%–17% larger than the sum of the Sn and Si covalent radii (2.58 Å), indicate a strong possibility of substantial Si relaxations. An earlier surface x-ray diffraction (SXRD) study of 1/3 ML Sn/Si(111)-$\sqrt{3}$ calculated that the adsorption of Sn produced considerable atomic relaxations within the first six sublayers of the Si substrate.[27] Similar vertical Si displacements were determined in a theoretical full-potential linearized augmented plane wave (FLAPW) study[28] and in an electron standing wave (ESW) structural study.[29] In the SXRD investigation, it was calculated that the Si atoms within the first substrate layer experiences a lateral displacement of 0.211 Å towards the Sn adatom. Incorporating these relaxations with the XSW-determined Sn time-averaged distribution results in a more realistic estimate for the Sn—Si bond lengths (from 3.01 Å to 2.86 Å for the upper Sn atoms and from 2.84 Å to 2.68 Å for the lower Sn atoms).

Beyond providing a more realistic picture of the Sn bonding arrangement, significant Si relaxations may have other consequences as well. The SXRD study calculated a large strain energy of 2.29 eV per $\sqrt{3}$ surface unit cell due to the stretching of Si bonds.[27] Some of this strain energy may be relieved by the substitution of Sn from the adatom layer into the Si substrate. While this phenomenon has not been directly observed by STM images of Sn/Si(111), STM has shown Si can substitute for Sn atoms in the adatom layer.[30] Furthermore, small shifts of Sn adatoms from the T_4 site were interpreted as the effect of substitutional Sn defects located in the first two Si layers. Finally, in a second set of XSW measurements on a second Sn/Si(111) sample, the substrate was annealed at 933 K for 2 min after depositing 0.45 ML of Sn, producing a sharp $\sqrt{3}$ LEED pattern and a final Sn coverage of 0.33(4) ML. While the annealing temperature used for this sample was not significantly higher than the annealing conditions for the 0.23 ML Sn/Si surface, the initial Sn coverage was increased by 36% over the first sample. This was done to compensate for Sn desorption during the annealing process in our attempt to come close to the ideal Sn coverage of 1/3 ML. As we will show in the following section, direct-space XSW images generated from this surface clearly demonstrate Sn can substitute for Si surface atoms incorporated in the Si(111) substrate.

The results of the XSW measurements collected on this 0.33 ML Sn/Si(111) surface are shown in Table II. As before, the coherent positions for the off-normal measurements can be compared with the (111) coherent position in order to deduce the in-plane structure of the Sn atomic distribution. The applicable geometric symmetry relationships for Sn atoms located at T_4 sites are $P_{022} = (4P_{111} - 1)/3$ and $P_{\bar{1}33} = P_{311} = (5P_{111} - 1)/3$. The off-normal XSW measurements on the higher-coverage surface do not obey these requirements, unlike the previously discussed XSW results. Furthermore, a comparison of the (111) and (333) XSW measurements shows $P_{333} = 0.71$ to be much greater than $\mathrm{Mod}[3P_{111}] = 3(0.71) - 2 = 0.13$, indicating a Sn atomic distribution that is markedly different from the one discussed earlier. Because a sufficient number of Fourier coefficients were measured on this higher-coverage Sn/Si(111)-$\sqrt{3}$ surface, the XSW direct-space imaging technique can be used to qualitatively probe where this difference arises without relying on a particular structural model.

TABLE II. Summary of the XSW results for the 0.33(4) ML Sn/Si(111) surface. The unit cell origin coincides with the top of the bulklike Si bilayer. XSW direct-space images of this surface show a significant fraction of the ordered Sn atoms have substituted for Si atoms below the adlayer.

(hkl)	P_H	f_H
(111)	0.71(1)	0.54(1)
(333)	0.71(3)	0.17(3)
(0 2 2)	0.09(1)	0.51(3)
$(\bar{1}\ 3\ 3)$	0.74(4)	0.15(5)
(3 1 1)	0.57(2)	0.24(3)

The XSW direct-space image generated from the XSW parameters in Table II is shown in Fig. 4. The increased in-plane width of the Sn atomic density distribution is partly due to the lower in-plane sensitivity of the off-normal XSW

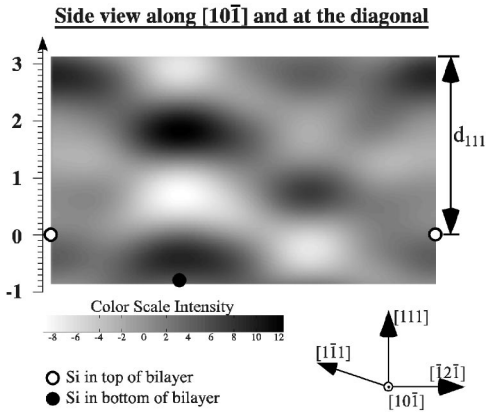

FIG. 4. XSW direct space Sn atomic density image for the Sn/Si(111)-$\sqrt{3}$ surface. The scale of the atomic density map directly results from evaluating Eq. (1) using the XSW data from Table II. A total of 0.45 ML of Sn was deposited on the Si(111) surface before annealing at 933 K. The coverage after annealing was 0.33(4) ML. While the majority of Sn appears adsorbed at the T_4 site, a significant amount appears to occupy a third site directly below the T_4 site within the Si surface.

measurements made for this surface. Above the Si surface, this image is quite similar to the XSW direct-space image from the lower-coverage surface shown in Fig. 3, since both indicate a Sn atomic density maximum close to 1.80 Å above the top of the Si bilayer. However, the image in Fig. 4 displays an additional Sn maximum that is approximately 25% smaller than the upper maximum and is located 0.35 Å below the top bilayer bulklike Si atoms. The two maxima are separated by 2.15 Å, and therefore are easily distinguished from each other in the XSW direct-space image, which has an expected resolution of 0.52 Å ($d_{333}/2$). Both atomic density maxima are centered on T_4 adsorption sites; therefore, the image suggests the surface incorporated Sn replaces Si atoms located in the bottom of the surface bilayer.

In order to quantitatively determine the amount and location of the subsurface Sn, the previously discussed structural model can be modified by introducing two additional parameters: c_{sub}, the fraction of ordered Sn that has migrated beneath the Si surface, and h_{sub}, the depth below the top of the Si bulklike bilayer to where the Sn has migrated. One constraint imposed on the Sn population is the fraction of ordered Sn located at T_4 sites $(1-c_{\mathrm{sub}})$ is fixed in a 1:2 occupation ratio. The previously described minimization routine can then be applied to the following equation for the *hhh* Fourier components:

$$F_m = f_m \exp(2\pi i P_m) = C \times [[(1 - c_{\mathrm{sub}})/3]\exp(2\pi i m h_A/d_{111}) + [2(1 - c_{\mathrm{sub}})/3]\exp(2\pi i m h_B/d_{111}) + (c_{\mathrm{sub}})\exp(2\pi i m h_{\mathrm{sub}}/d_{111})] \times \exp(-2\pi^2 m^2 \langle u^2\rangle / d_{111}^2). \quad (3)$$

When fitting this revised set of equations to the XSW data in Table II, the heights h_A and h_b as well as the thermal vibrational amplitude are fixed at the values determined from the previously discussed calculation ($h_A = 2.04$ Å, $h_B = 1.78$ Å, $\langle u^2\rangle^{1/2} = 0.13$ Å). After applying these constraints, the least-squares minimization routine returns a best fit in which 38% (±3%) of the ordered Sn is located 0.37(4) Å below the top of the Si bulklike surface. The fraction of Sn that is not randomly distributed is $C = 0.81(4)$.

A similar analysis can be used to quantify the amount of subsurface Sn for the 0.23 ML Sn/Si(111) surface. Reevaluating the XSW data for this surface determined only a small amount (6±3%) of the ordered Sn is located 0.5(1) Å below the ideal Si surface. The inclusion of subsurface Sn in our surface model did not significantly affect the other structural parameters. The reduced chi-squared value for this fit was 1.87.

To further assess if the chosen structural model is reasonable, we can compare the measured Sn fluorescence yield modulation with simulated Sn fluorescence yields based on our adsorption model. This comparison is shown in Fig. 2, which depicts the simulated Sn fluorescence as a dotted-dash line and the best fit to the measured Sn $L\alpha$ fluorescence as a solid line. There is good agreement between the measured Sn fluorescence yield and the calculated yield curves; therefore, our structural model can be considered a reasonable description of the Sn atomic arrangement. As further corroboration, recent XSW studies on Sn/Ge(111) (Ref. 31) also find a large amount of Sn (up to 20%) diffused into the Ge surface after annealing the Ge surface to a higher temperature.

Our "one-up, two-down" surface model can also be compared to the results of previous investigations of the Sn/Si(111)-$\sqrt{3}$ surface. In one such study, Profeta *et al.* predicted that Sn occupies a single adsorption height of 1.80 Å with respect to the top of the Si bulklike layer.[28] This study mentioned the possibility of multiple adatom heights. Another study by Yamanaka *et al.* used ESW to determine a single Sn adsorption height of 2.06 Å with respect to the top of the Si bulklike layer.[29] However, it was also proposed that Sn could also be located in two inequivalent sites. Molecular dynamics simulations were used to calculate a vertical separation between two Sn sites of 0.3 Å. This calculation was used to reanalyze the ESW data, which produced a Sn height distribution with maxima at 1.96 Å and 2.26 Å, with the maximum at 1.96 Å being 30% larger than the upper maximum. Neither study addressed the possibility of Sn incorporation in the Si surface. These earlier single-height models are compared with our XSW-derived model in Fig. 2, which shows the calculated Sn fluorescence yield curves from the conclusions of Profeta *et al.* and Yamanaka *et al.* as dotted and dashed lines, respectively. It is clear from this comparison that our multiple-adsorption height model best matches the measured Sn fluorescence yield from the 0.23 ML Sn/Si(111) surface.

It is also important to consider other possible explanations for the observed vertical Sn asymmetry other than the dynamical fluctuations model. First and foremost, we can consider the effect of the presence of defects in the Sn/Si(111) surface. In the specific case of the low coverage surface, the most obvious defect is the amount of Sn is smaller than the ideal 1/3 ML coverage. This raises the question of whether the asymmetric height distribution observed by XSW is caused by this reduced coverage. For Sn on Si(111), the $\sqrt{3}$ phase is stable over a wide coverage range (0.16–0.33 ML),[23] unlike in the Sn on Ge case. This is because Si adatoms will occupy the T_4 sites that would be filled by Sn adatoms if the coverage were closer to 0.33 ML. Therefore, instead of considering the effect of Sn surface vacancies on the observed Sn distribution, it is more useful to consider the effect of Si adatoms located in T_4 sites. A recent angle-resolved photoemission study examined the effect of Sn coverage on the electronic band structure of the $Si_xSn_{(1-x)}$/Si(111) $\sqrt{3}$ phase.[21] It found that the electronic structure is constant as a function of coverage in the 0.23–0.33 ML range, signifying the dangling bonds of the intermixed Si adatoms behave similarly to the Sn dangling bonds and there is no significant charge transfer between the two types of atoms. This finding suggests the influence of neighboring Si adatoms on the Sn vertical distribution is small, as least from an electronic standpoint.

IV. CONCLUSION

In conclusion, it has been experimentally determined that Sn adatoms are arranged in a "one up, two down" configuration, with one-third of the Sn at 2.04 Å above the top of

the ideal Si bilayer and two-thirds at 1.78 Å. This Sn distribution is similar to the atomic distribution measured by XSW of the $\sqrt{3}$ phase and (3×3) phase of Sn/Ge(111). This similarity supports a dynamical fluctuations model of the Sn/Si(111) surface, in which Sn atoms move in a correlated fashion between two unique adsorption sites. This atomic arrangement presents an underlying (3×3) structure, as expected from previous core-level and valence-band photoemission studies and as observed in the isoelectronic 1/3 ML Sn/Ge(111) system. In a separate surface treatment, a higher initial coverage of Sn was deposited on Si(111). The measured Sn XSW Fourier coefficients were used to generate a model-independent 3D direct-space image, which unambiguously shows Sn migrating below the Si(111) surface and substituting for Si in the bottom of the surface bilayer.

ACKNOWLEDGMENTS

The authors thank P. Baldo and Z. Zhang for technical assistance, and M. Asta, T.-L. Lee, and E. Tosatti for helpful discussions. This work was supported by the NSF under Contract Nos. DMR-9973436 and DMR-0076097; and the DOE under Contract Nos. W-31-109-ENG-38 to ANL and DE-FG02-03ER15457 to NU.

[1] H. Morikawa, I. Matsuda, and S. Hasegawa, Phys. Rev. B **65**, 201308 (2002).
[2] J. M. Carpinelli, H. H. Weitering, M. Bartkowiak, R. Stumpf, and E. W. Plummer, Phys. Rev. Lett. **79**, 2859 (1997).
[3] J. M. Carpinelli, H. H. Weitering, E. W. Plummer, and R. Stumpf, Nature (London) **381**, 398 (1996).
[4] A. V. Melechko, J. Braun, H. H. Weitering, and E. W. Plummer, Phys. Rev. Lett. **83**, 999 (1999).
[5] A. V. Melechko, J. Braun, H. H. Weitering, and E. W. Plummer, Phys. Rev. B **61**, 2235 (2000).
[6] L. Petersen, Ismail, and E. W. Plummer, Phys. Rev. B **65**, 020101 (2002).
[7] H. H. Weitering, J. M. Carpinelli, A. P. Melechko, J. D. Zhang, M. Bartkowiak, and E. W. Plummer, Science **285**, 2107 (1999).
[8] T. E. Kidd, T. Miller, M. Y. Chou, and T. C. Chiang, Phys. Rev. Lett. **85**, 3684 (2000).
[9] J. Avila, A. Mascaraque, E. G. Michel, M. C. Asensio, G. LeLay, J. Ortega, R. Perez, and F. Flores, Phys. Rev. Lett. **82**, 442 (1999).
[10] D. Farias, W. Kaminski, J. Lobo, J. Ortega, E. Hulpke, R. Perez, F. Flores, and E. G. Michel, Phys. Rev. Lett. **91**, 016103 (2003).
[11] J. Ortega, R. Perez, and F. Flores, J. Phys.: Condens. Matter **14**, 5979 (2002).
[12] R. Perez, J. Ortega, and F. Flores, Phys. Rev. Lett. **86**, 4891 (2001).
[13] J. S. Okasinski, C.-Y. Kim, D. A. Walko, and M. J. Bedzyk, Phys. Rev. B **69**, 041401 (2004).
[14] R. I. G. Uhrberg, H. M. Zhang, and T. Balasubramanian, Phys. Rev. Lett. **85**, 1036 (2000).
[15] R. I. G. Uhrberg and T. Balasubramanian, Phys. Rev. Lett. **81**, 2108 (1998).
[16] H. T. Anyele, C. L. Griffiths, A. A. Cafolla, C. C. Matthai, and R. H. Williams, Appl. Surf. Sci. **123**, 480 (1998).
[17] M. Gothelid, M. Hammar, C. Tornevik, U. O. Karlsson, N. G. Nilsson, and S. A. Flodstrom, Surf. Sci. **271**, L357 (1992).
[18] L. Ottaviano, G. Profeta, L. Petaccia, S. Santucci, and M. Pedio, Surf. Sci. **501**, L171 (2002).
[19] R. I. G. Uhrberg, H. M. Zhang, T. Balasubramanian, S. T. Jemander, N. Lin, and G. V. Hansson, Phys. Rev. B **62**, 8082 (2000).
[20] A. Charrier, R. Perez, F. Thibaudau, J. M. Debever, J. Ortega, F. Flores, and J. M. Themlin, Phys. Rev. B **64**, 115407 (2001).
[21] J. Lobo, A. Tejeda, A. Mugarza, and E. G. Michel, Phys. Rev. B **68**, 235332 (2003).
[22] G. Ballabio, G. Profeta, S. de Gironcoli, S. Scandolo, G. E. Santoro, and E. Tosatti, Phys. Rev. Lett. **89**, 126803 (2002).
[23] C. Tornevik, M. Göthelid, M. Hammar, U. O. Karlsson, N. G. Nilsson, S. A. Flodström, C. Wigren, and M. Ostling, Surf. Sci. **314**, 179 (1994).
[24] M. J. Bedzyk and L. W. Cheng, in *Reviews in Mineralogy and Geochemistry*, edited by P. Fenter *et al.* (Mineralogical Society of America, Washington, 2002), Vol. 49, p. 221.
[25] L. Cheng, P. Fenter, M. J. Bedzyk, and N. C. Sturchio, Phys. Rev. Lett. **90**, 255503 (2003).
[26] Z. Zhang, P. Fenter, L. Cheng, N. C. Sturchio, M. J. Bedzyk, M. L. Machesky, and D. J. Wesolowski, Surf. Sci. **554**, L95 (2004).
[27] K. M. Conway, J. E. Macdonald, C. Norris, E. Vlieg, and J. F. Vanderveen, Surf. Sci. **215**, 555 (1989).
[28] G. Profeta, A. Continenza, L. Ottaviano, W. Mannstadt, and A. J. Freeman, Phys. Rev. B **62**, 1556 (2000).
[29] T. Yamanaka and S. Ino, Phys. Rev. B **61**, R5074 (2000).
[30] S. T. Jemander, N. Lin, H. M. Zhang, R. I. G. Uhrberg, and G. V. Hansson, Surf. Sci. **475**, 181 (2001).
[31] J. S. Okasinski, Ph.D. thesis, Northwestern University, 2003).